Harnessing icIEF to Unlock Protein-Based Therapeutics

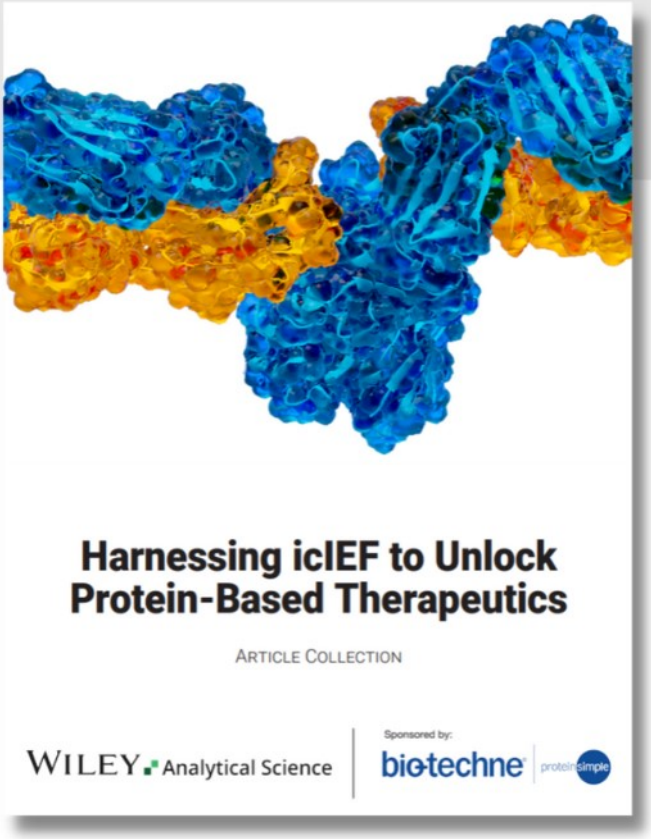

Read the new Article Collection

Keep up to date with the latest developments in biotherapeutics and the range of treatments for various diseases with our latest article collection. Find out how imaged cIEF (icIEF) technique is essential for quality control and analytical development of these drugs, as it accurately determines the surface charge of lipid nanoparticles and the charge heterogeneity of proteins and antibodies.

This article collection aims to provide you with more information on these techniques and technologies, helping you further your research in this field.

bio-techne® | protein simple

WILEY

ADVANCED HEALTHCARE MATERIALS
www.advhealthmat.de

Dual-Targeted Nanoparticle-in-Microparticle System for Ulcerative Colitis Therapy

Yawen Zhang, Yue Wu, Yuping Yan, Yijing Ma, Linglan Tu, Jingjing Shao, Xuanyu Tang, Lingfeng Chen, Guang Liang, and Lina Yin**

Conventional oral therapy for ulcerative colitis (UC) is associated with premature release or degradation of drugs in the harsh gastrointestinal environment, resulting in reduced therapeutic effectiveness. Consequently, the present study aims to develop a dual-targeted delivery system with a nanoparticle-in-microparticle (nano-in-micro) structure. The prepared Asiatic Acid-loaded delivery system (AA/CDM-BT-ALG) has pH-sensitive properties. Cellular uptake evaluation confirms that nanoparticles exhibit targeted absorption by macrophages and Caco-2 cells through mannose (Man) receptor and biotin-mediated endocytosis, respectively. Therefore, this mechanism effectively enhances intracellular drug concentration. Additionally, the biodistribution study conducted on the gastrointestinal tract of mice indicates that the colon of the microspheres group shows higher fluorescence intensity with longer duration than the other groups. This finding indicates that the microspheres exhibit selective accumulation in areas of colon inflammation. In vivo experiments in colitis mice showed that AA/CDM-BT-ALG significantly alleviates the histopathological characteristics of the colon, reduced neutrophil, and macrophage infiltration, and decreases pro-inflammatory cytokine expression. Furthermore, the effect of AA/CDM-BT-ALG on colitis is validated to be closely related to the TLR4/MyD88/NF-κB signaling pathway. The present findings suggest that the development of a dual-targeted delivery system is accomplished effectively, with the potential to serve as a drug-controlled release system for treating UC.

1. Introduction

Ulcerative colitis (UC) is an inflammatory bowel disease with a high risk of developing colon cancer. The pathological features of UC include a disrupted epithelial barrier and inflammatory dysregulation in the colon.[1] The first-line therapies of UC typically involve using anti-inflammatory medications, immunosuppressants,[2,3] and biological agents.[4,5] The oral route is the most suitable approach for UC patients due to its high safety and compliance. However, the bioavailability of most drugs after oral administration is low, resulting in inadequate efficacy. This is mainly due to three major problems: 1) Low efficiency in targeting inflammatory sites; 2) The drug absorption limitation in the intestine owing to the transmembrane transport barrier of intestinal epithelial cells; 3) The drug degradation and destruction due to the acidic environment in the stomach (pH 1.0–2.5) and pepsin. Unfortunately, current studies have focused on one or two of these barriers,[6,7] with limited attention given to overcoming the three obstacles of oral UC treatment.

During the UC pathological process, many macrophages are activated and highly expressed in the colon.[8,9] The Man receptor is an effective endocytic carbohydrate-binding receptor,[10] which is overexpressed on the macrophage surface.[11,12] Therefore, polymeric micelles modified with the Man group can be used as macrophage-targeting molecules that specifically accumulate in the inflammation site.[13,14] Additionally, the negatively charged lipid bilayer on the intestinal cell surface acts as a natural barrier that limits drug entry into the cells. Biotin, a water-soluble vitamin, is essential for normal cell growth and is actively absorbed by epithelium via sodium-dependent multivitamin transporter (SMVT). Conjugates with biotin can improve intestinal cell permeability and increase drug absorption.[15,16] Alignate (ALG), a nontoxic and biodegradable polyanionic polymer, is used to control drug release due to its unique pH sensitivity and high degradation rate. Hence, ALG is a promising material for colon targeting.[17,18] Therefore, we hypothesized that ALG-coated Man-biotin dual-modified polymer microspheres might be an intelligent oral targeted delivery system for UC.

Y. Zhang, Y. Wu, Y. Yan, Y. Ma, X. Tang, L. Chen, G. Liang, L. Yin
School of Pharmacy
Hangzhou Medical College
182 Tianmushan Rd, Hangzhou 310013, China
E-mail: 2020000411@hmc.edu.cn; lnyin@hmc.edu.cn
L. Tu
School of Laboratory Medicine and Bioengineering
Hangzhou Medical College
Hangzhou 310013, China
J. Shao
School of Pharmacy
Wenzhou Medical University
Wenzhou 325000, China

The ORCID identification number(s) for the author(s) of this article can be found under https://doi.org/10.1002/adhm.202301518

DOI: 10.1002/adhm.202301518

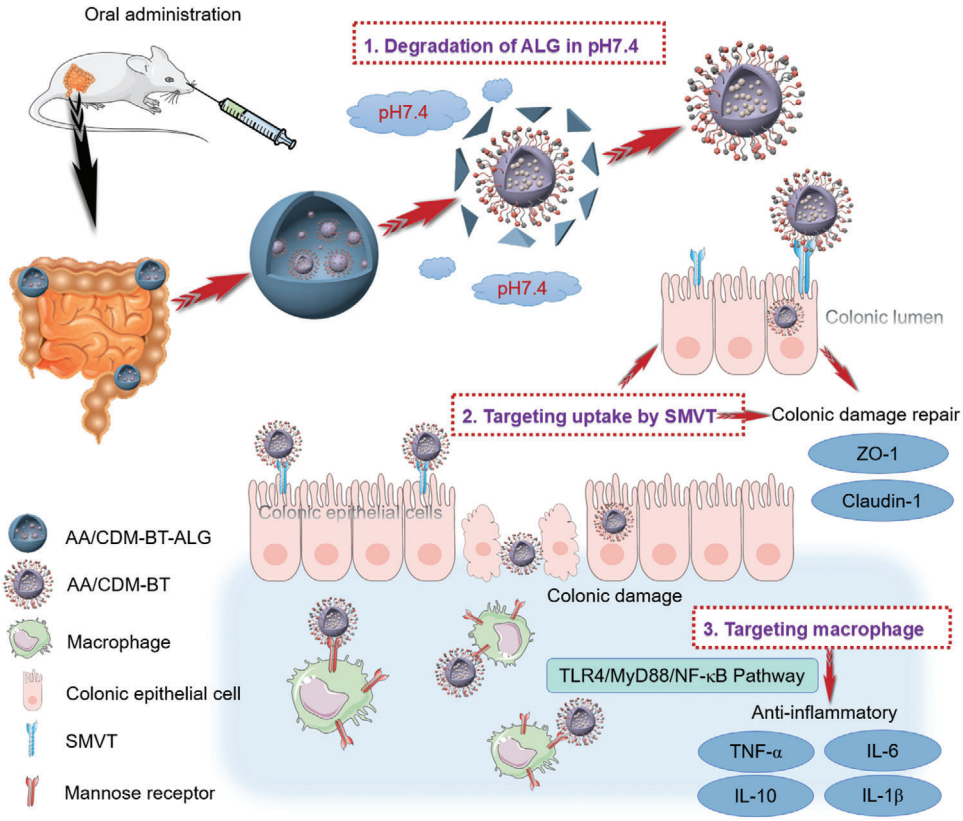

Scheme 1. Schematic illustration of the dual-targeted nanoparticle-in-microparticle system in the treatment of UC[a]. [a]1) The ALG shell of AA/CDM-BT-ALG microspheres dissolves in the intestinal environment and releases nano-micelles in the colon. 2) Bio-TPGS micelles transmembrane into cells by targeting SMVT-mediated endocytosis in the intestinal tract. 3) CS-DCA-Man micelles target macrophages at inflammatory sites and inhibit inflammatory factors through the TLR4/MyD88/NF-κB signaling pathway, thereby treating UC.

Natural products have been used to treat colitis for centuries and represent the first choice for complementary and alternative UC therapy. Asiatic acid (AA), a pentacyclic triterpene acid isolated from the medicinal plant *Centella Asiatica*, exhibits anti-inflammatory, antioxidant, and anticancer effects.[19–21] Additionally, AA could protect mice against Lipopolysaccharide (LPS)-induced acute lung injury,[22] liver injury,[23,24] and acute pancreatitis.[25] Consequently, we hypothesized that AA might have a therapeutic effect on UC. However, the clinical application of AA is minimal owing to its low water solubility, rapid elimination in vivo, short half-life, and extremely low oral bioavailability.[26,27]

To address this unmet medical need, we propose a novel dual-targeted strategy to effectively increase the oral absorption of anti-colitis drugs; **Scheme 1** shows the hypothesis of this study. First, two micelles were prepared using Man-modified chitosan-deoxycholic acid (CS-DCA-Man) and biotin-modified D-α-Tocopherol polyethylene glycol 1000 succinate (Bio-TPGS) as polymer-carriers to target macrophages at inflammatory sites and increase SMVT-mediated endocytosis in intestinal epithelial cells. Then calcium ALG microspheres (AA/CDM-BT-ALG) with the nano-in-micro structures were further prepared to deliver the loaded AA to the intestinal tract as much as possible (**Figure 1**A). The targeted absorption effect, drug release characteristics, and anti-UC efficacy were thoroughly assessed in vitro and in vivo. Moreover, the mechanism of AA and its drug delivery system in colonic inflammatory diseases through the TLR4/MyD88/NF-κB signaling pathway was first explored in this article.

2. Experimental Section

2.1. Materials

AA (98%) was supplied by the Guangxi Institute for Food and Drug Control (Guangxi, China). Chitosan (CS, deacetylation degree > 89.1%) with an average molecular weight of 126 kDa was acquired from Golden-shell Biochemical Co., Ltd. (Zhejiang, China). Near-infrared fluorescent dyes C6 and DiR were purchased from Dalian Meilun Biotechnology Co., Ltd. (Liaoning, China). Deoxycholic acid (DCA), Biotin, D-α-Tocopherol polyethylene glycol 1000 succinate (TPGS), sodium ALG (viscosity 200 ± 20 mpa.s), and dextran sodium sulfate (DSS) were obtained from Aladdin (Shanghai, China). α-D-Mannopyranosylphenyl isothiocyanate was acquired from Beijing Chemsynlab Co., Ltd. (Beijing, China). LPS and 1-ethyl-3-(dimethyl aminopropyl) carbodiimide hydrochloride (EDC·HCl) were procured from Sigma-Aldrich (St. Louis, USA). Toll-like receptor 4 (TLR4), myeloid differentiation factor 88 (MyD88), and NF-κB p65 antibodies were procured from Abcam (Cambridge, MA). p-NF-κB-p65(Ser 536) antibodies were procured

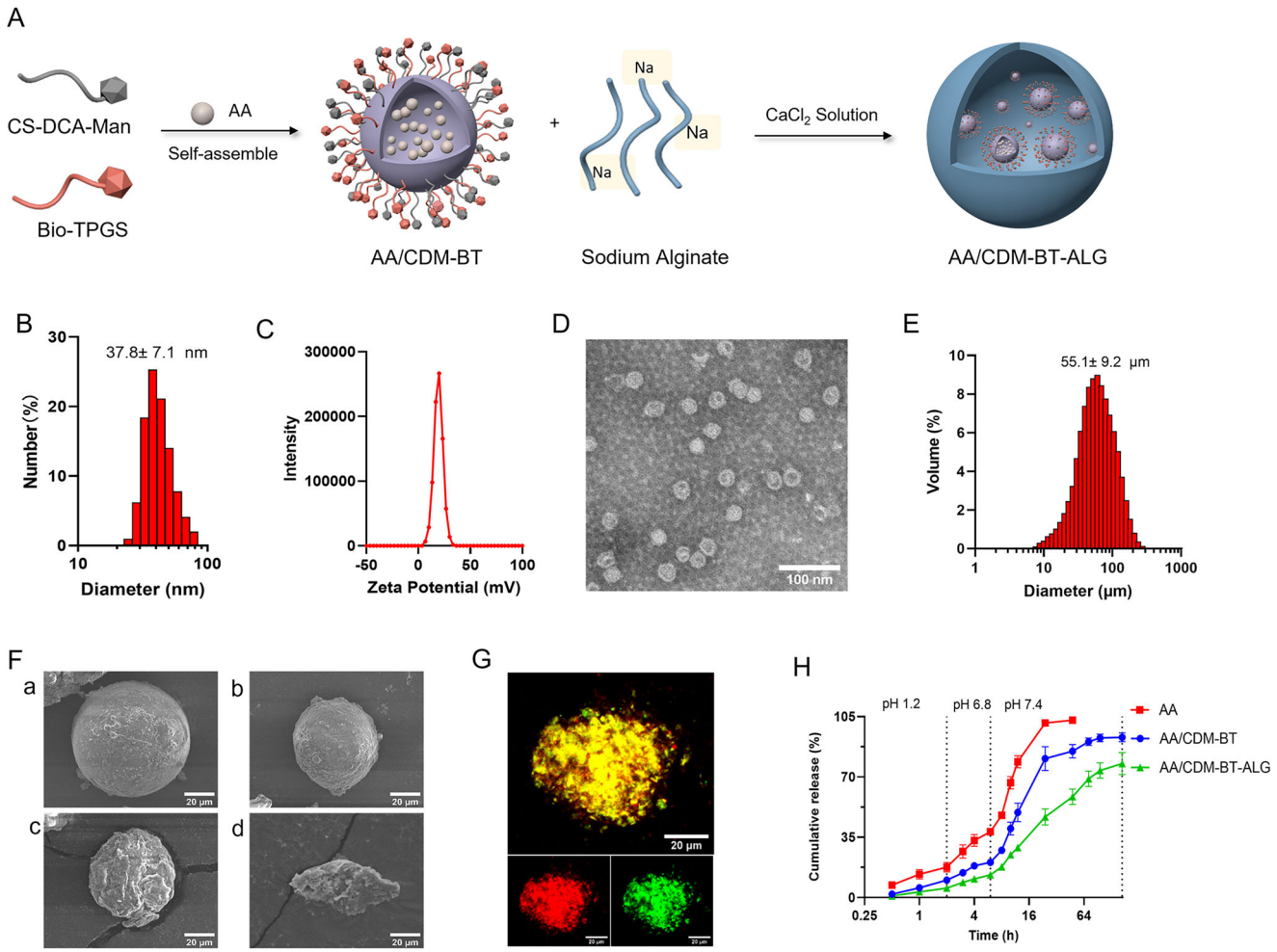

Figure 1. Characterization and drug release profiles of nano-micelles and microspheres. A) The structure of AA-loaded nano-in-micro delivery system (AA/CDM-BT-ALG) with dual-targeted properties. B) The size distribution of AA/CDM-BT (4^{th} prescription). C) The zeta potential of AA/CDM-BT (4^{th} prescription). D) TEM images of AA/CDM-BT (4^{th} prescription). Scale bar = 100 nm. E) The size distribution of AA/CDM-BT-ALG. F) Scanning electron microscope (SEM) images of AA/CDM-BT-ALG soaked in different media. Scale bar = 20 μm. G) Fluorescence microscopy images of AA/CDM-BT-ALG. Scale bar = 20 μm. H) In vitro release profiles of free AA, AA/CDM-BT, and AA/CDM-BT-ALG in simulated gastrointestinal conditions ($n = 3$). Each point represents the mean ± SD.

from Affinity Biosciences (Jiangsu, China). BCA protein assay kit and 3-(4,5-Dimethylthiazol-2-21-yl)−2,5-diphenyl tetrazolium bromide (MTT) were obtained from Beyotime Biotechnology Co., Ltd. (Shanghai, China). All other solvents and reagents were of analytical grade.

2.2. Preparation and Characterization of CS-DCA-Man and Bio-TPGS

2.2.1. Synthesis of CS-DCA

CS-DCA was synthesized according to the reported method.[28] Briefly, 4.5 g DCA and 6.6 g EDC·HCl were prepared by being dissolved in a mixed solvent of acetone and ethanol and were then activated by stirring for 1 h. Subsequently, the solution was added to 500 mL aqueous CS and stirred overnight at 60°C. The CS-DCA was acquired by dialysis (7000 Da) and vacuum drying.

2.2.2. Synthesis of CS-DCA-Man

Figure S1A, Supporting Information, presents the chemical reaction scheme of CS-DCA-Man. Briefly, 30 mL distilled water was used to dissolve 1 g of CS-DCA and mixed with 150 mg Man in 7.5 mL DMSO. The mixture was subjected to 24 h of magnetic stirring at room temperature in darkness. Ultimately, CS-DCA-Man was obtained by dialysis against water for 24 h and freeze-drying. The acquired pellets were determined using ^{1}H-NMR (AC-80, Brucker Biospin Co., Germany).

2.2.3. Synthesis of Bio-TPGS

Bio-TPGS was synthesized by linking the carboxyl group of biotins and the hydroxyl group of TPGS using DMAP and EDC·HCl as catalysts (Figure S1C, Supporting Information). Briefly, 60 mL anhydrous DMSO was used to dissolve 1.5 g biotin,

0.6 g DMAP, and 1.2 g EDC·HCl. The carboxyl groups in biotin were activated by stirring for 6 h at room temperature. Then, 3.0 g TPGS was added and stirred in darkness for three days. After two days of dialysis with distilled water (1000 Da), the Bio-TPGS powder was obtained by freeze-drying, confirming its structure using ^{1}H-NMR.

2.3. Preparation and Characterization of Nanoparticles

The AA-loaded nanoparticles (AA/CDM-BT) were prepared by solvent evaporation. The aqueous solutions of CS-DCA-Man and Bio-TPGS were prepared with 5 mg mL^{-1} final concentrations. As Table S1, Supporting Informationshows5 mg mL^{-1} AA in ethanol was added to the mixed solution of each formulation with stirring (600 rpm) at room temperature. Ethanol was removed using decompression evaporation while removing unencapsulated AA by centrifugation at 3000 rpm (AnkeGL-20G-II, Shanghai, China). The supernatant represented the AA/CDM-BT micelles of prescriptions 1–7.

The mean particle size, polydispersity index (PDI), and surface zeta potential of AA/CDM-BT dispersion were measured using Malvern Zetasizer Nano ZS90 after five-fold dilution with distilled water and ultrasonic dispersion (400 W, work for 2s, stop for 3s, 3 min) (JY92-2D, Scientz Biotechnology Co. Ltd., China). The particle morphology was photographed by transmission electron microscopy (TEM) (FEI Tecnai F30, USA).

The AA content of AA/CDM-BT was determined using HPLC on a Shimadzu LC-20AD system.[24] The mobile phase composition comprised KH_2PO_4 (pH 3.0) and methanol/acetonitrile (1:1) at a 20/80 volume ratio with a 1.0 mL min^{-1} flow rate. The UV detector was set at 210 nm wavelength. The centrifuged AA/CDM-BT dispersion was 25-fold diluted with methanol-acetonitrile (1:1), then ultrasonicated for 10 min, and the filtrate was collected for HPLC detection. The encapsulation efficiency (EE, %) and drug loadings (DL, %) of AA were determined as follows:

$$\mathrm{EE}(\%) = \frac{\text{Amount of drug in AA/CDM} - \text{BT}}{\text{Total drug added}} \times 100\% \quad (1)$$

$$\mathrm{DL}(\%) = \frac{\text{Amount of drug in AA/CDM} - \text{BT}}{\text{Weight of AA/CDM} - \text{BT}} \times 100\% \quad (2)$$

Fluorescently labeled nanoparticles were prepared by replacing AA with C6 or DiR (C6/CDM-BT and DiR/CDM-BT), which were used in cell uptake and in vivo distribution experiments, respectively.

2.4. Preparation and Characterization of the Nano-in-Micro Delivery System

The AA/CDM-BT was encapsulated in ALG microspheres to generate AA/CDM-BT-ALG, thereby protecting the drug release in the stomach and anterior small intestine. Briefly, 2% ALG solution was added dropwise to 2% Span 80 solution and emulsified with mechanical stirring (400 rpm) in 2 h of 40 °C water bath. Next, the AA/CDM-BT dispersion (4th prescription) was added slowly and stirred for 15 min. Then, 10% calcium chloride solution was added and cross-linked for 3 h. After the mixed solution was centrifuged (9000 rpm) for 10 min, petroleum ether was used to wash the precipitate four times, which was then vacuum-dried overnight to obtain AA/CDM-BT-ALG microspheres. Fluorescently labeled microspheres were prepared using C6 or DiR in place of AA (C6/CDM-BT-ALG and DiR/CDM-BT-ALG) for fluorescence imaging.

The particle size distribution of AA/CDM-BT-ALG was measured using a laser particle size analyzer (Malvern 2000, UK). The micro-morphology of AA/CDM-BT-ALG was investigated using scanning electron microscope (SEM) (IT200, JEOL, Japan). Microspheres samples were covered with gold and scanned under an accelerating voltage of 15 kV. The final AA loading of AA/CDM-BT-ALG was calculated based on Equation 3. The dried AA/CDM-BT-ALG was quantitatively weighed and placed in 5% w/v sodium citrate solution, ultrasonicated for 10 min, and heated for 40 min. Subsequently, 1.5 mL ethanol was added to extracted AA, followed by 10 min of sonication and 3 h of 60 °C heating. Finally, the mixture was centrifuged, and the AA content in the microspheres was determined using HPLC as described above.

$$\mathrm{DL}(\%) = \frac{\text{Amount of drug in microspheres}}{\text{Weight of microspheres}} \times 100\% \quad (3)$$

To investigate drug release behavior, dialysis bags (MW 7000 Da) were filled with AA solution, nano-micelle dispersion (AA/CDM-BT), and microspheres (AA/CDM-BT-ALG) (equivalent to 1 mg AA). These dialysis bags were placed in 20 mL of HCl solution (pH 1.2, 1% SDS) and shaken at 100 rpm at 37 °C. After 2 h, the dialysis bags were transferred to 20 mL of phosphate buffer (pH 6.8, 1% SDS), followed by 37 °C incubation for another 6 h. Afterward, the release medium was changed to pH 7.4 PBS with 1% SDS. Then, the medium removal beside 20 mL replenishment with fresh medium took place at predetermined time points. All samples were centrifuged (10 000 rpm, 5 min), and AA was detected by the HPLC method described above. The sampling intervals were 0.5, 1, 2, 3, 4, 6, 8, 10, 12, and 24 h as well as 2, 3, 4, and 7 days.

The morphological changes of microspheres during drug release was further investigated. AA/CDM-BT-ALG was soaked in pH 1.2 HCl solution, pH 6.8 PBS, and pH 7.4 PBS for 2 h, respectively. Then the residual particles were removed, sprayed with gold, and observed under SEM.

2.5. Cytotoxicity Assay

An MTT assay was utilized with Raw 264.7 macrophages and Caco-2 cells to evaluate the cytotoxicity of AA and AA/CDM-BT micelles. Raw 264.7 macrophages and Caco-2 cells were seeded into 96-well plates (6×10^3 cells per well) and incubated at 37 °C for 24 h, respectively. Next, the cells were incubated with gradient concentrations (4, 10, 25, and 50 μM) of AA or AA micelles (seven prescriptions) for 24 h at 37 °C. Subsequently, MTT solution (5 mg mL^{-1}, 20 μL) was added to each well and incubated for another 4 h. Afterward, 200 μL DMSO was added to completely dissolve the formazan crystals. The OD490 values of each well were recorded by a microplate reader (Synergy2, Bio-Tek, USA). Cells untreated with drugs represented 100% viability.

2.6. Cellular Uptake of AA/CDM-BT

Effective cellular uptake is a vital prerequisite for drug efficacy. To further determine the optimal ratio of double micelles in AA/CDM-BT, the cellular uptake of the seven prescriptions of fluorescently labeled micelles (C6/CDM-BT) in Raw 264.7 macrophages and Caco-2 cells using C6 as a fluorescent probe was studied. Raw 264.7 macrophages and Caco-2 cells were seeded onto 12-well plates (2×10^5 cells per well) to quantify the cell uptake of various prescriptions and cultured for 12 h. Cells were then incubated with C6 or C6/CDM-BT suspension (seven prescriptions) at a final C6 concentration of 10 μg mL^{-1} at 37 °C; Table S1, Supporting Information, lists the seven formations. After incubation for 5, 15, 30, 60, and 120 min, the cells were thoroughly washed with PBS at 4 °C to remove unassociated micelles. Then, cell lysate was added, and the samples were freeze-thawed at −80 °C three times. The fluorescence intensity of C6 and the protein concentrations of Raw 264.7 macrophages and Caco-2 cells in centrifuged supernatant were measured by a microplate reader (Synergy2, Bio-Tek, USA).

Furthermore, to investigate the functional targeting of micelles, Raw 264.7 macrophages, and Caco-2 cells were seeded onto 12-well plates at the same density and steps described above. After 12 h of cell adhesion, Raw 264.7 were preincubated with 5 mg mL^{-1} biotin for 2 h, and Caco-2 cells were preincubated with 5 mg mL^{-1} Man. Then, the 1st, 4th, and 7th prescriptions were added and co-inducted for another 2 h. The rest operations are the same as described above.

Additionally, to compare uptake properties visually, Raw 264.7 macrophages and Caco-2 cells were seeded onto 12-well plates with glass discs at the same density as above. Similarly, after culturing for 12 h, Raw 264.7 macrophages and Caco-2 cells were presaturated with biotin or Man solution. Then, C6/CDM-BT micelles (10 μg mL^{-1}, 1st, 4th, or 7th prescriptions) were added and incubated for another 2 h. Cells were fixed with 4% paraformaldehyde for 15 min and stained with Hoechst 33 258 (nucleus dye, 10 μg mL^{-1}) and DiI (cell membrane dye, 10 μg mL^{-1}) for 10 min, respectively. The glass disc was inverted onto a glass slide and observed under an Axiocam 503 mono microscope camera (Zeiss) with an X-Cite 120 Q fluorescence Light Source (Excelitas technologies, USA) with a 20× objective.

2.7. In Vitro Anti-Inflammatory Activities of AA/CDM-BT

Raw264.7 macrophages were used to examine the AA/CDM-BT anti-inflammatory influence. Cells were seeded into 12-well plates (2×10^5 cells per well) and incubated in a complete medium for 12 h. After preincubating with AA or AA/CDM-BT at the concentration of 25 μM for 1 h, LPS (1 μg mL^{-1}) was added and incubated for 24 h. The negative control group was unstimulated with LPS. The cell supernatants were collected to detect inflammatory factors.

2.8. Induction of UC Mouse Model

Male Balb/c mice (18–22 g) were procured from Zhejiang Laboratory Animal Center (Hangzhou, China) and housed at 22–25 °C in a 12/12 h light/dark cycle. All animal care and experiments followed the laboratory animal care principles and were approved by the Animal Ethics Committee of Zhejiang Province (2021–095). Three cycles were used to induce the chronic colitis model, each containing 3% DSS for seven days, followed by seven days of water drinking (Figure 6A).

2.9. In Vivo Intestinal Absorption Characteristics

The absorption characteristics of the nano-in-micro system in different intestinal segments in vivo were further evaluated. Briefly, the duodenum, jejunum, ileum, and colon of mice were separated. Subsequently, they were ligated at both ends (≈2 cm) and infused with C6/CDM-BT or C6/CDM-BT-ALG (10 μg mL^{-1}). The intestinal segments were washed with saline and collected after 2 h. The frozen slices were stained by DAPI and photographed under a fluorescence scanner (3DHISTECH, PANORAMIC SCAN II). The fluorescence intensity of each group was calculated using Image J.

2.10. Bio-Distribution in Colitis Mice

To study the in vivo targeting properties of nanoparticles and microspheres, near-infrared dye DiR was used as a fluorescent probe. Mice with colitis were allocated randomly into three experimental groups ($n = 9$ per group). They were orally given free DiR, DiR-loaded nanoparticles (DiR/CDM-BT), and DiR-loaded microspheres (DiR/CDM-BT-ALG) at a DiR dose of 3 mg kg^{-1}. Mice were euthanized 6, 12, and 24 h after drug administration, and the five major organs (the heart, liver, spleen, lung, kidney) and entire gastrointestinal tract were collected and photographed using an in vivo imaging system (IVIS) (Lumina III, Caliper, USA). The fluorescence signal of DiR-loaded formulations was visible at $\lambda\ E_x$ 720 nm and $\lambda\ E_m$ 790 nm wavelengths.

2.11. In Vivo Therapeutic of AA/CDM-BT-ALG in Colitis Mice

After one week of feeding adaptation, the Balb/c mice were categorized randomly into four groups ($n = 6$ per group): 1) Normal group (healthy mice without DSS), 2) Model group (DSS-induced colitis mice without drug), 3) AA group (DSS-induced colitis mice orally administered AA with a daily dose of 30 mg kg^{-1}), and 4) AA/CDM-BT-ALG group (DSS-induced colitis mice orally administered AA/CDM-BT-ALG daily, equal to 30 mg kg^{-1} AA). Throughout the experiment, animal body weight, visible stool consistency, and fecal bleeding twice a week were monitored. The disease activity index (DAI) was utilized to comprehensively evaluate colitis severity in mice, including the comprehensive evaluation of weight loss (0–4), stool consistency state (1–3), and fecal bleeding (1–3).[29] Body weight loss score was as follows: 0, < 1%; 1, 1%–5%; 2, 5%−10%; 3, 10%−15%; 4, > 15%. The stool consistency score was as follows: 1) well-shaped particles; 2) mushy and semi-formed stools, not sticking to the anus; 3) loose stools that stick to the anus. Bleeding score: 1) no bleeding; 2) recessive bleeding; 3) severe bleeding. The mice were euthanized at the end of the experiment, and the entire colon (from cecum to anus)

and the five major organs were excised and photographed. Corresponding colon sections were isolated for histological analysis and to determine cytokine levels. Blood samples were collected to determine cytokine levels using corresponding ELISA kits.

2.11.1. Pathological Evaluation

Histological analysis of mice colon tissues was performed using Hematoxylin-Eosin (H&E) and Periodic acid-Schiff (PAS) staining to evaluate the therapeutic effect of AA/CDM-BT-ALG on colitis. The distal colons and the five main organs in each group were fixed in 4% paraformaldehyde at ambient temperature, sectioned into slices, and stained with H&E or PAS. Sections were viewed with a fully automatic digital slide scanning system (NIKON, ECLIPSE E100). The colitis severity in each colonic segment was evaluated blindly by assessing mucosal characteristics, including epithelium damage, inflammatory cell infiltration, and goblet cell loss.

2.11.2. Immunohistochemical Staining

Paraffin-embedded colon sections were deparaffinized, hydrated, and antigen-extracted. Subsequently, 3% H_2O_2 was used to quench the endogenous peroxidase for 10 min. Moreover, 5% bovine serum albumin was utilized to perform section blocking for 20 min. Then, anti-ZO-1 (1:1500, Wuhan Sanying Biotechnology Co., Ltd.) and anti-claudin-1 (1:200; Wuhan Sanying Biotechnology Co., Ltd.) were added and incubated overnight at 4 °C, followed by 2 h of incubation with secondary antibody IgG (Tuling Hangzhou Biomedicine Co., Ltd.). DAB was added to the sections to visualize positive cells.

2.11.3. Immunofluorescence Assay of Neutrophils and Macrophages

Immunofluorescence staining was performed on colitis tissue to assess neutrophil and macrophage infiltration at inflammation sites. Briefly, paraffin-embedded colon samples were cut into 5 µm-thick sections and then dewaxed with xylene and gradient alcohol solution. After repairing in EDTA antigen repair buffer (pH 8.0), sections were blocked for 30 min at 25 °C with 3% bovine serum albumin. Furthermore, tissue sections were incubated with primary polyclonal anti-myeloperoxidase (MPO, 1:1000, Abcam, Cambridge, UK; F4/80, 1:400, Cell Signaling Technology, Beverly, MA USA) overnight at 4 °C, followed by 1 h incubation with horseradish peroxidase-conjugated goat-anti-rabbit secondary antibody (Hangzhou Haoke Biotechnology Co., Ltd, China) at 25 °C. Finally, colon sections were stained with 10 µg mL^{-1} DAPI and analyzed using an inverted fluorescence microscope (ECLIPSE C1, NIKON).

2.11.4. Evaluation of Pro-Inflammatory Cytokines in Colon Tissue

Besides neutrophil and macrophage infiltration at colonic inflammation sites, key pro-inflammatory cytokines, including interleukin-6 (IL-6), tumor necrosis factor-α (TNF-α), interleukin-10 (IL-10), and interleukin-1β (IL-1β), were secreted.[30] Therefore, to estimate the therapeutic effect of AA/CDM-BT-ALG on DSS-induced colitis mice, ELISA kits (Invitrogen, California, USA) were used to detect inflammatory cytokines in the colon tissue and serum of each group. Briefly, colon sections were cultured in serum-free RPMI 1640 medium with penicillin/streptomycin for 24 h. Subsequently, ELISA was used to analyze IL-6, TNF-α, IL-10, and IL-1β concentrations in the supernatant per the protocols. The data were reported as pg/mg tissue protein. Total protein concentration was detected using the BCA kit (Fisher Scientific, Waltham, MA, USA). Additionally, IL-6 and TNF-α concentrations in serum were measured.

2.12. Real-Time Polymerase Chain Reaction Analysis

The gene expression of inflammatory factors in macrophage supernatant and colon tissue was identified using RT-PCR. The total mRNA in Raw 264.7 cells and tissues was extracted and purified using the SteadyPure RNA Extraction Kit (Accurate Biotechnology (Hunan) Co., LTD), determining its concentration using a NanoDrop2000 spectrophotometer (Thermo Scientific, Waltham, MA, USA). The β-actin, IL-6, TNF-α, IL-10, and IL-1β gene expressions were measured by SYBR-based quantitative PCR analysis (Hieff qPCR SYBR Green Master Mix, Yeasen Biotech Co., Ltd, Shanghai, China) using a programmed My Cycler (BIO-RAD, Germany). The thermocycling conditions were 95 °C for 30 s, followed by 40 cycles of 95 °C for 5 s, and 60 °C for 30 s. Melting curve conditions were 95 °C for 40 s, dropping the temperature to 60 °C in 1 min. **Table 1** lists the used sequences of primers. The data were analyzed using the comparative $2^{-\triangle\triangle Ct}$ method in quadruplicate.

2.13. Western Blotting Analysis

The pathogenesis of UC is reported to be closely related to the immune system. TLR4 is an innate immune receptor that activates the NF-κB inflammatory signaling pathway through MyD88, leading to inflammatory cytokine secretion, thus contributing to colitis progression.[31,32] Western blotting was used to analyze TLR4, MyD88, and NF-κB p65 expressions in colon tissue. The total protein was extracted using a RIPA lysis kit (Beyotime, Shanghai, China) and quantified using a BCA assay kit (Beyotime, Shanghai, China). SDS-PAGE was used to separate the samples, which were transferred to a PVDF membrane (Millipore) and blocked for 1.5 h in a 5% BSA solution. The specimens were then incubated with the primary antibodies overnight at 4 °C, followed by 1 h incubation with the secondary antibodies at 25 °C. The β-actin antibodies were used as internal controls. The obtained chemiluminescence signals were quantified by Image J software.

2.14. Statistical Analysis

Statistical analysis was conducted using a one-way variance analysis (ANOVA) followed by a Bonferroni post hoc test (GraphPad Prism 9.0). Data are reported as mean ± SD. Statistical differences were defined as * $p < 0.05$, ** $p < 0.01$, *** $p < 0.001$, **** $p < 0.0001$, and ns indicates nonsignificant.

Table 1. Sequences of the primers used in RT -PCR analysis.

Gene	Forward primer sequence (5′−3′)	Reverse primer sequence (5′−3′)
β-actin (mouse)	CCGTGAAAAGATGACCCAGA	TACGACCAGAGGCATACAG
TNF-α (mouse)	TGATCCGCGACGTGGAA	ACCGCCTGGAGTTCTGGAA
IL-6 (mouse)	GAGGATACCACTCCCAACAGACC	AAGTGCATCATCGTTGTTCATACA
IL-10 (mouse)	GGTCTGAGTGGGACTCAAGG	CGTGGCAATGATCTCAACAC
IL-1β (mouse)	AGGTCGTCATCATCCCACGAG	GCTGTGGCAGCTACCTATGTCTTG

3. Results and Discussion

3.1. Characterization of CS-DCA-Man and Bio-TPGS

CS-DCA-Man was synthesized by reacting the amine group of CS with the carboxyl group of DCA and the isothiocyanate group of a-D-mannopyranyl isothiocyanate, respectively (Figure S1A, Supporting Information). The product structure was determined by ^{1}H-NMR (Figure S1B, Supporting Information). The feature peaks of CS can be seen in three compounds: CS, CS-DCA, and CS-DCA-Man at δ 1.9 (–$COCH_3$) and δ 2.9–4.9 (six hydrogens on the benzene ring). Three methyl peaks of DCA at δ 0.6, 0.8, and 0.9 are observed in DCA and CS-DCA. Furthermore, the DCA carboxy proton peak at δ 12 is observed in neither CS nor CS-DCA, indicating the DCA grafting onto CS. The characteristic peaks of Man include δ 7.0–7.2 for hydrogen on the benzene ring and δ 5.5 for acetal on the sugar ring. These chemical shifts are also observed in CS-DCA-Man, suggesting the successful grafting of Man.

Figure S1D, Supporting Information, illustrates that the chemical shift value of δ 0.80 is the hydrogen on the methyl group in the vitamin E succinate structure in TPGS. The peaks observed within the chemical shift range of δ 1.00–1.70 corresponds to the signal produced by the methylene hydrogen in vitamin E succinate. Additionally, the peaks at δ 1.86, 1.88, and 1.97 are the hydrogen atoms present in the benzene ring of vitamin E. Finally, the peak at δ 2.47 is indicative of the methylene group located at the 4-position of the chroman ring in vitamin E. The hydrogen signal peaks of δ at 2.66 and 2.85 are the two methylene groups on the succinate chain of TPGS. Meanwhile, the signal peak at 3.47 belongs to the methylene group on the polyethylene glycol chain in the structure. Compared to the TPGS spectra, Bio-TPGS exhibited additional peaks, specifically at δ 2.34 (2H, brs), 3.10 (1H, brs), 4.32 (1H, m), and 6.35–6.40 (2H, =N–H, brs).[33,34] These peaks represent the characteristic proton peak of biotin, ensuring that the grafting of biotin onto the TPGS skeleton was successfully achieved.

3.2. Characterization of AA/CDM-BT

The physicochemical properties of the seven formulated micelles were evaluated, including particle size distribution, PDI, zeta potential, EE, and DL, providing the results in Table S1, Supporting Information. The micelles were prepared with small particle sizes ranging from 20–140 nm, and the PDI was less than 0.4, indicating good dispersion. The increased CS-DCA-Man ratio in the formulation increases the zeta potential, possibly related to the positive CS charge. The EE and DL of the seven prescriptions were above 90% and 10%, respectively. This result indicated that the solvent evaporation method was suitable for preparing AA micelles. A comprehensive comparison showed that the particle size of the 4th prescription was moderate (37.8 ± 7.1 nm) (Figure 1B), with the highest EE (99.3 ± 7.5%) and DL (13.0 ± 1.0%). Additionally, the zeta potential of the 4th prescription was greater than 20 mV (21.9 ± 1.6 mV) (Figure 1C), which was considered stable and preliminarily selected for further research. TEM images of the 4th prescription (Figure 1D) showed that the micelles were spherical with a narrow particle size distribution, consistent with the PDI values measured by Malvern.

3.3. Characterization of AA/CDM-BT-ALG

ALG-based microcarriers were designed to efficiently deliver AA to the colon to protect the entrapped AA from being degraded in the acid environment of the stomach and then released in the neutral intestinal region. The particle size distribution and morphology of AA/CDM-BT-ALG were investigated by laser particle analyzer and SEM, respectively. The results showed that AA/CDM-BT-ALG exhibited a spherical appearance with a particle size of 55.1 ± 9.2 μm (Figure 1E,F). Furthermore, Coumarin 6 (C6)-labeled micelles and Rhodamine-labeled microspheres were prepared and observed under confocal laser scanning microscopy (CLSM, LSM710, Zeiss). The images revealed that the microspheres were spherical, and the fluorescent nanoparticles were evenly wrapped into the microspheres. This observation verified that microspheres were successfully prepared with nano-in-micro structures (Figure 1G). The loaded AA was quantitatively determined by HPLC, and the results showed that the EE was 8.3 ± 1.0%.

The release profiles of AA, AA/CDM-BT, and AA/CDM-BT-ALG in vitro were performed at 37°C in hydrochloric acid, pH 6.8 and pH 7.4 buffer, corresponding to gastric juice, intestinal juice (duodenum, colon), respectively. As Figure 1H shows that the AA cumulative release in the pH 1.2 solution was nearly 20% after 2 h, reaching the endpoint of 101.2% within 24 h. Moreover, AA is not released rapidly in an acidic medium, probably because the pKa of AA was ≈4.7, resulting in low solubility in acid, thereby affecting the release rate. AA/CDM-BT micelles could slow AA release, with 10.1% and 20.4% released at 2 and 6 h, respectively, and the release was completed within 4 days with 92.6%. The cumulative release of AA/CDM-BT-ALG microspheres in pH 1.2 solution for 2 h was only 5.4%, lower than that of AA/CDM-BT micelles. This result indicated that ALG and AA/CDM-BT formed a tight structure that could protect the encapsulated drug in an acidic environment. This phenomenon revealed that ALG

exhibited colon-targeting function. In the acidic environment of the stomach, the calcium ALG on the outer layer of AA/CDM-BT-ALG microspheres is converting into alginic acid, covering the microspheres surface to form a dense protective layer, reducing drug release.[35] When AA/CDM-BT-ALG reaches the intestinal tract, the alginic acid on the microspheres outer layer forms water-soluble ALG, and the microspheres rupture to release the encapsulated AA/CDM-BT micelles, which further releases the drug slowly.[30] Under the action of Bio-TPGS and CS-DCA-Man, the drug was targeted and accumulated in the inflamed tissue, increasing intestinal absorption via SMVT endocytosis.

Additionally, the morphological stability and pH-dependent degradation of AA/CDM-BT-ALG were evaluated using SEM. Figure 1E illustrates that AA/CDM-BT-ALG remained completely spherical after soaking in a pH 1.2 solution for 2 h, which may be due to the shrinkage of the alginic acid in the outer layer of microspheres into a dense structure under an acidic environment. However, in the pH 6.8 buffer, the microspheres outer layer was disrupted. Interestingly, the morphology of the microspheres became irregular after 2 h in pH 7.4 buffer, indicating that the outer layer was dissolved.

3.4. Cytotoxicity

The cytotoxicity of AA and AA/CDM-BT were detected using the MTT method, with the AA concentration of 4–50 μM. As shown in **Figure 2**A, LPS stimulation did not affect cell viability (102%). The cell viability values of AA and AA micelles (seven prescriptions) in Raw 264.7 macrophages were higher than 80% of the control group after 24 h, indicating that AA/CDM-BT had no special toxicity. Similar results were found for Caco-2 cells (Figure 2B). This indicated that the constructed micellar delivery system had good biocompatibility and was safe for oral administration.

3.5. Intracellular Uptake of AA/CDM-BT

Cell internalization is a crucial prerequisite for drugs to exert their biological functions. The cellular uptake efficiency of micelles with different formulations on Raw 264.7 cells and Caco-2 cells was quantitatively determined at 5, 15, 30, 60, and 120 min, respectively. As Figure 2C shows, increasing the time from 5 to 120 min increased C6 fluorescence intensity in the seven prescriptions. This increase indicated that C6/CDM-BT uptake by Raw 264.7 cells is time-dependent. After incubation for 2 h with the seven prescriptions, the fluorescence of the 1st prescription was the highest, followed by the 4th ($p < 0.01$). This evidence strongly supported that Man contributed to the increased macrophage uptake rate of CS-DCA-Man; this result was further confirmed, as shown in Figure 2E. The preincubation of Raw 264.7 cells with free Man rapidly reduced the fluorescence intensity of C6/CDM-BT compared to nonincubated micelles ($p < 0.01$). The same time-dependent results were observed in Caco-2 cells (Figure 2D). Of all the prescription micelles, the 7th prescription showed the highest fluorescence intensity, possibly due to the effective uptake of biotin-modified Bio-TPGS via the SMVT pathway.[36] Interestingly, fluorescence intensity between the 4th and 7th prescriptions showed an insignificant difference ($p > 0.05$). Conversely, C6/CDM-BT exposure to Caco-2 cells preincubated with free biotin, which binds to the receptor site on the Caco-2 cell surface in advance, resulted in a significant decrease in intracellular fluorescence of the 4th and 7th prescriptions ($p < 0.001$) (Figure 2F). These results supported the active role of biotin in the targeted absorption of enterocytes, facilitating the intracellular uptake of therapeutic drugs. The results revealed the ability of surface functionalization with Man or biotin to improve the cellular uptake efficacy of micellar particles by Raw 264.7 or Caco-2 cells. After conducting a comprehensive comparison of the absorption characteristics of each formulation in the two cell lines, it could be concluded that the 4th prescription exhibited superior performance. Therefore, the 4th prescription micelles were selected for subsequent experiments.

Furthermore, fluorescence microscopy was used to observe the intracellular uptake of micelles in Raw 264.7 and Caco-2 cells after 2 h incubation. The positions of the nucleus (blue fluorescence), cell membrane (red fluorescence), and C6 (green fluorescence) were analyzed (Figure 2G), showing the internalization of different micelles formulations by macrophages and Caco-2 cells. Caco-2 cell results showed that the intracellular fluorescence of 1st, 4th, and 7th prescriptions was strong. After adding Man, the intracellular fluorescence value in the 1st prescription remained significantly unchanged. This phenomenon indicated that the uptake process in intestinal cells of 1st prescription micelles primarily depended on the excellent adhesion properties and intestinal epithelial absorption promoting effect of CS-DCA,[28] while Man had little effect. However, Bio-TPGS uptake decreased significantly after biotin presaturation in the 7th prescription, suggesting that the uptake mechanism of Bio-TPGS in Caco-2 is related to the biotin-mediated endocytosis.

Interestingly, the uptake capacity of three prescriptions in Raw 264.7 cells was weaker than in Caco-2 cells. Therefore, a competitive cellular uptake study was conducted to verify whether biotin induced a higher therapeutic effect. Figure 2G presents that C6/CDM-BT exhibited moderate-intensity green fluorescence in macrophages. However, the cellular uptake of C6/CDM-BT was drastically reduced in the presence of free Man. Conversely, the fluorescence intensity remained significantly unchanged upon biotin addition. These findings implied that C6/CDM-BT enters cells via the Man receptor on the macrophage surface. Quantitative and qualitative analysis affirmed the internalizing effect of biotin on intestinal cells and the targeting ability of Man on macrophages, validating that the nano-system had dual targeting properties.

3.6. Anti-Inflammatory Activity of AA/CDM-BT in Cells

The number of pro-inflammatory cytokines throughout UC shows high elevation.[37] **Figure 3** illustrates that the mRNA expression levels of IL-6, IL-1β, and TNF-α of Raw 264.7 macrophages were significantly increased after LPS treatment for 24 h. Moreover, inflammatory factor levels decreased slightly in cells treated with free AA and significantly in the AA/CDM-BT treatment group. These results are consistent with in vitro cell uptake studies. Additionally, the inflammatory cytokine down-regulation in the AA/CDM-BT group may be related to

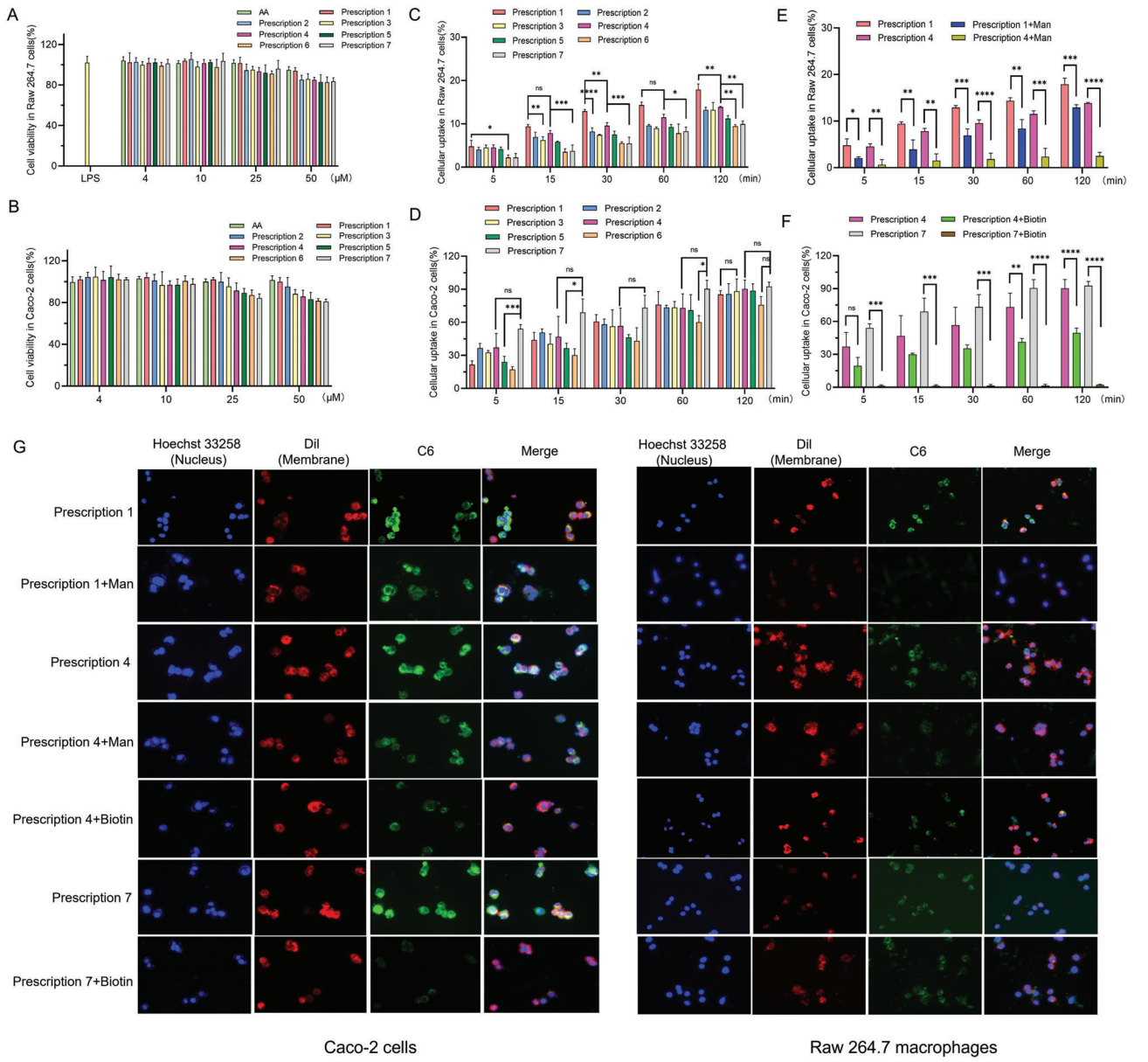

Figure 2. Cytotoxicity and uptake properties evaluation in vitro. Cytotoxicity evaluation of AA and AA/CDM-BT against Raw 264.7 macrophages A) and Caco-2 cells B) following 24 h of co-incubation based on MTT assays ($n = 5$). Quantitative uptake properties of micelles with different formulations in Raw 264.7 C) and Caco-2 cells D) ($n = 3$). E) Quantitative uptake of AA/CDM-BT micelles in Raw 264.7 macrophages pre-saturated with Man ($n = 3$). F) Quantitative uptake of AA/CDM-BT micelles in Caco-2 cells pre-saturated with biotin ($n = 3$). G) Fluorescence microscopy images of cell internalization profiles of AA/CDM-BT micelles with different formulations in two cell lines pre-saturated with biotin or Man. Each point represents the mean ± SD. * $p < 0.05$; ** $p < 0.01$; *** $p < 0.001$; **** $p < 0.0001$; ns, no significant difference.

biotin-modified nanomaterials.[38] Biotin can reduce inflammatory cytokine expression, including TNF-α, thereby treating inflammatory diseases.[39]

3.7. Intestinal Absorption Evaluation

The release and accumulation of drugs in the colon region is a crucial feature of effective UC treatment. **Figure 4** shows that the fluorescence intensity of the four intestinal segments had little difference after enteral perfusion of C6/CDM-BT, indicating no difference in micelles absorption in the intestinal tract. Interestingly, only weak fluorescence was observed in the duodenum after infusion of C6-labeled microspheres, demonstrating little drug release and absorption. However, the fluorescence intensity in the colonic region was significantly higher than in the other intestinal segments. It was confirmed that the microspheres shell was destroyed in this region, and most micelles were released into the colon and absorbed by colon cells. Altogether, the nano-in-micro system exhibited apparent pH sensitivity and a colon-targeting effect.

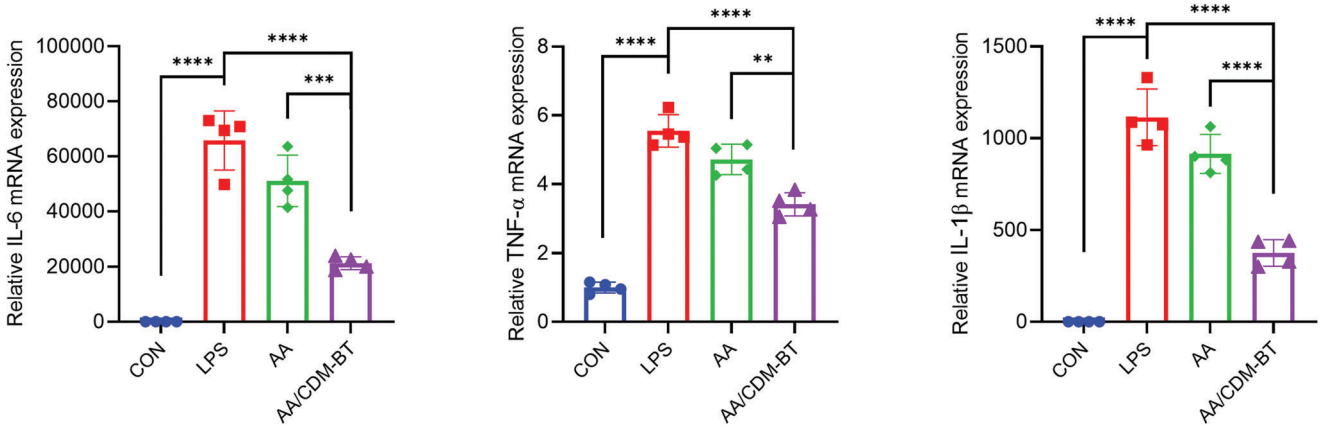

Figure 3. In vitro anti-inflammatory activities of AA and AA/CDM-BT against Raw 264.7 macrophages. IL-6, TNF-α, and IL-1β mRNA expression levels were quantified by real-time polymerase chain reaction (RT-PCR) ($n = 4$). Each point represents the mean ± SD. ** $p < 0.01$; *** $p < 0.001$; **** $p < 0.0001$.

3.8. In Vivo Biodistribution Evaluation

Targeted accumulation of therapeutic agents in colon tissue is essential for UC oral treatment. DiR, DiR-loaded micelles (DiR/CDM-BT), or DiR-loaded microspheres (DiR/CDM-BT-ALG) were administered orally to mice with colitis, and IVIS obtained images to assess the ability of colon-specific delivery. Strong fluorescence appeared in the stomach after intragastric administration of free DiR to mice (**Figure 5**). Then the fluorescence gradually moved to the intestinal tract, weakening the fluorescence intensity. After 24 h, slight fluorescence was detected due to absorption or excretion. Mice showed a strong fluorescence intensity in the stomach 6 h after DiR/CDM-BT administration. This might reflect either the release of drug-loaded micelles or unabsorbed DiR in the stomach. Moreover, the fluorescence intensity gradually increased as the micelles converged in the colon at 12 h, whereas a small amount of fluorescence was still visible in the cecum and colon after 24 h. These observations indicated that DiR was slowly released from the micelles, and the retention time in vivo was longer than that of the free DiR group. However, the fluorescence of the cecum and colon in the DiR/CDM-BT-ALG group was more elevated than in the DiR/CDM-BT group at 6, 12, and 24 h (Figure 5A,C). This suggested that the calcium ALG microspheres protected the encapsulated micelles and prevented premature drug release in the stomach.

Additionally, due to the biological adhesion of ALG,[40,41] the drug residence time in the intestinal tract can be prolonged. The decomposition of the calcium ALG microspheres shell in the intestinal tract releases the micelles, thereby releasing the drug slowly. Therefore, it can precisely deliver and release the drug to the inflammatory site of the colon. This in vivo profile was similar to the release profiles of AA/CDM-BT and AA/CDM-BT-ALG in different pH buffers (Figure 1H). Meanwhile, the fluorescence

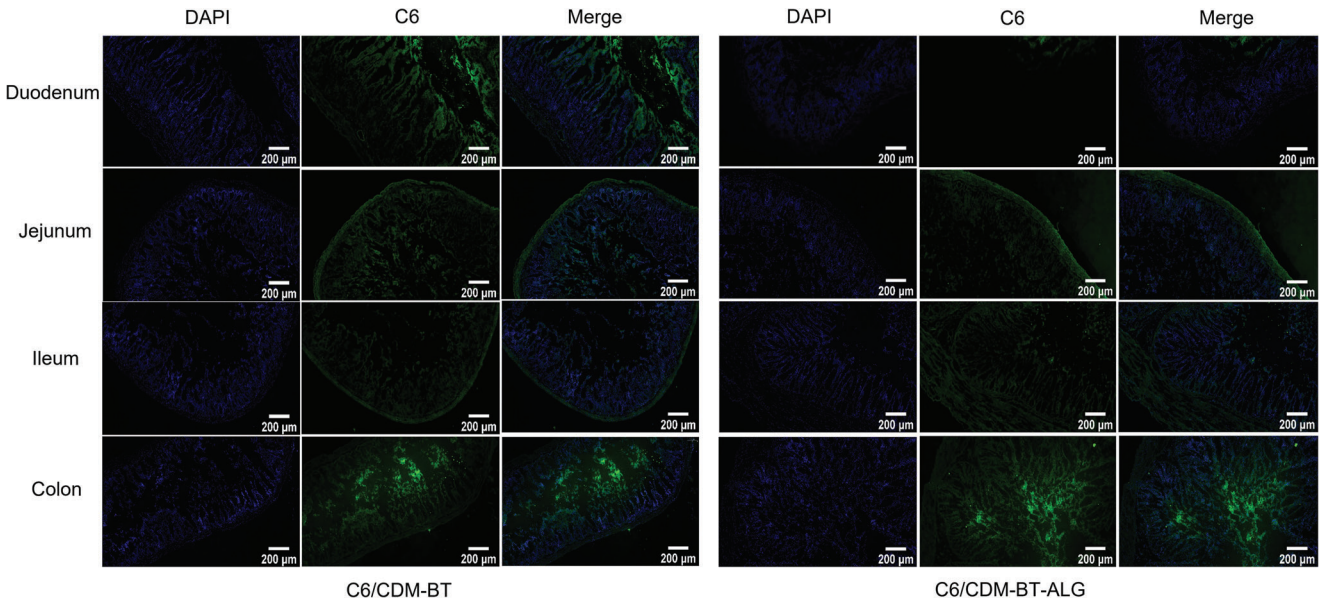

Figure 4. Fluorescence images of different intestinal segments. Scale bar = 200 μm.

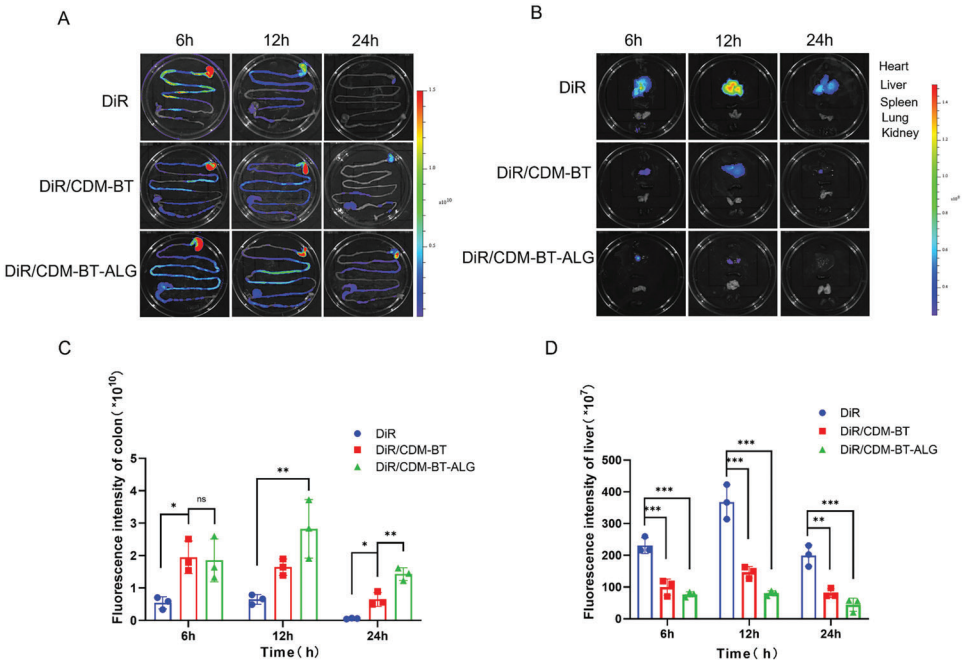

Figure 5. In vivo bio-distribution evaluation of DiR-loaded nanoparticles and microspheres after oral administration to mice. A) IVIS images of DiR, DiR/CDM-BT, and DiR/CDM-BT-ALG in different segments of mice gastrointestinal tract at various time points (6, 12, and 24 h). B) Fluorescence images of the major organs in mice. Fluorescence intensities were quantified and compared in the colon C) and liver D) at 6, 12, and 24 h post-dosing ($n = 3$). Each point represents the mean ± SD. * $p < 0.05$; ** $p < 0.01$; *** $p < 0.001$; ns, no significant difference.

intensity in the mouse colon at various time points was measured by IVIS images (Figure 5C). The fluorescence intensity of DiR/CDM-BT-ALG microspheres in the colon was significantly stronger than the free drug group ($p < 0.05$), indicating the accumulation of drugs in colitis tissues.

The biodistribution characteristics of nanoparticles and microspheres were studied by tracking the DiR signal in mice. Figure 5B demonstrates the arrangement of five main organs at 6, 12, and 24 h, and Figure 5D shows the quantitative statistics of the liver. There was strong fluorescence in the liver after oral administration of free DiR. However, only weak fluorescence was observed in the kidney, with no distribution in other organs. Due to the targeting effect of CS-DCA-Man and Bio-TPGS, the fluorescence intensity of DiR/CDM-BT micelles decreased in the liver while increasing in the intestinal tract. The contribution of ALG resulted in a further increased accumulation of DiR/CDM-BT-ALG microspheres in the colon site, resulting in decreased fluorescence in the liver. These results confirmed that the prepared calcium ALG microspheres could specifically accumulate in colon tissue after oral administration.

3.9. In Vivo Therapeutic Efficiency of AA/CDM-BT-ALG Against UC

The DSS-induced mice model is a typical UC animal model with similar pathological features to humans, including body weight loss, shortened colon, colonic epithelial layer destruction, and inflammatory cell infiltration.[42] Therefore, the anti-inflammatory effect of AA/CDM-BT-ALG was performed in DSS-induced colitis mice. First, we assessed weight loss, a recognized phenotypic indicator of colitis. **Figure 6**B illustrates that the body weight of normal mice continued to increase during the experiment while the model group fluctuated significantly. This could be due to intestinal injury caused by DSS oral administration, resulting in weight loss in the model group. Following drug withdrawal, the body weight recovered slightly. By the end of the experiment (Day 42), the weight gain was ≈13.5% of the control group and −5.3% of the model group. The body weight in the daily oral administration of the AA/CDM-BT-ALG group was greater than that of the AA group, indicating a better curative effect on UC recovery. Compared to normal mice, the DAI of DSS-treated mice was significantly increased, and the colon was shortened (Figure 6C-E). Conversely, AA/CDM-BT-ALG-treated mice exhibited lower DAI and significantly preserved colon length. Overall, AA/CDM-BT-ALG-treated mice showed the least weight loss and the best weight recovery among the treated groups.

The histological effect of AA/CDM-BT-ALG against UC was evaluated by H&E staining. Figure 6F-G shows that the colon sections of healthy mice showed insignificant inflammation or destruction. However, the model group showed vital signs of inflammation, including epithelial erosion (black arrows), goblet cell loss (green arrows), crypt destruction, and a large number of inflammatory cells in the lamina propria (yellow arrows). According to histological analysis, all treatment groups showed a specific effect. The colon tissue of the AA treatment group was slightly reduced than the model group. Nevertheless, there were still some signs of ulceration, including moderate damage to the epithelial tissue and partial inflammatory cell infiltration. Conversely, the AA/CDM-BT-ALG group morphology was almost normal, with only slight inflammation, low cellular infiltration, and highly conformal crypt, indicating that the abnormal changes of diseased

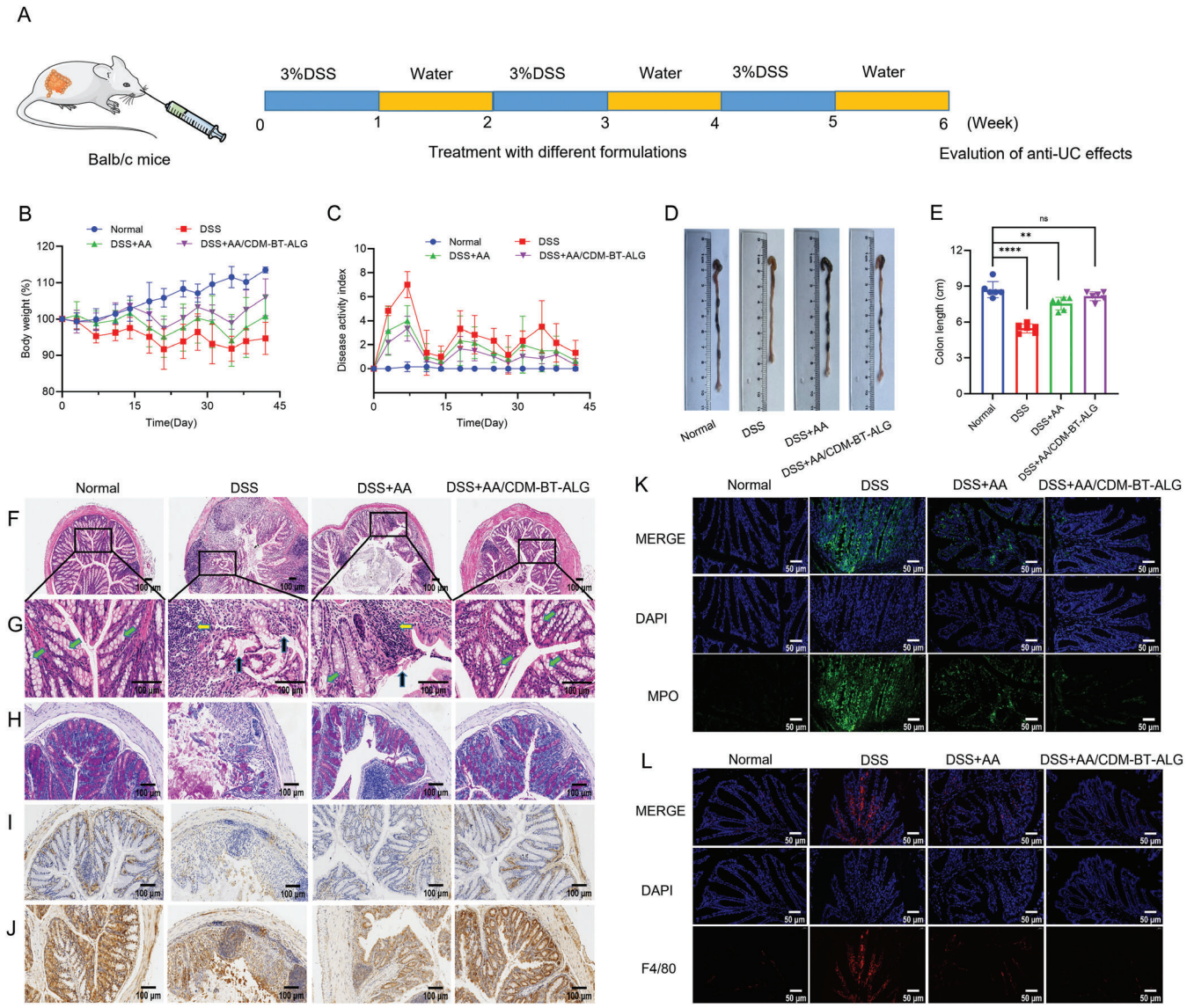

Figure 6. In vivo therapeutic outcomes of AA/CDM-BT-ALG against UC. A) Schematic diagram of colitis induction and treatment. B) Time-dependent variations of body weights normalized as a percentage of day-0 body weight ($n = 6$). C) DAI scores ($n = 6$). D) Photographs of the colons of different groups. E) Quantitative analysis of colon length among different formulations ($n = 6$). F, G) Representative H&E staining images of colon tissues from different groups (10 ×, F; 40 ×, G). (Black arrows, epithelial erosion; green arrows, loss of goblet cells; yellow arrows, inflammatory cells). Scale bar = 100 μm. H) Representative PAS staining images of colon tissues. I) Immunohistochemical analysis of ZO-1 and J) Claudin-1. Immunostained colon sections illustrate K) neutrophil infiltration (Green, neutrophils; Blue, DAPI for nuclear staining), and L) macrophage infiltration into the mucosa (Red, macrophages (F4/80); Blue, DAPI for nuclear staining). Scale bars = 50 μm. Each point represents the mean ± SD. *$p < 0.05$; **$p < 0.01$; ns, no significant difference.

colon tissue were effectively improved. Collectively, the in vitro and in vivo data indicate that AA/CDM-BT-ALG can effectively promote UC recovery.

Additionally, we preliminarily evaluated the potential side effects of AA/CDM-BT-ALG treatment. Notably, H&E pathological examination of the main organs of treated mice showed no pathological changes (Figure S2, Supporting Information), which confirmed the safety of oral administration of AA/CDM-BT-ALG and provided a prerequisite for potential clinical transformation.

3.10. Protective Effect of AA/CDM-BT-ALG on the Colonic Barrier

The intestinal epithelial barrier is vital in UC progression. Colonic goblet cells produce and secrete mucus to maintain the mucosal barrier of the colon. Here, we evaluated goblet cell abundance in colon sections using PAS staining. Figure 6H shows that, compared to normal cells, the goblet cells in the model group were severely lost, and the number of intact cells was reduced. However, the AA/CDM-BT-ALG microspheres

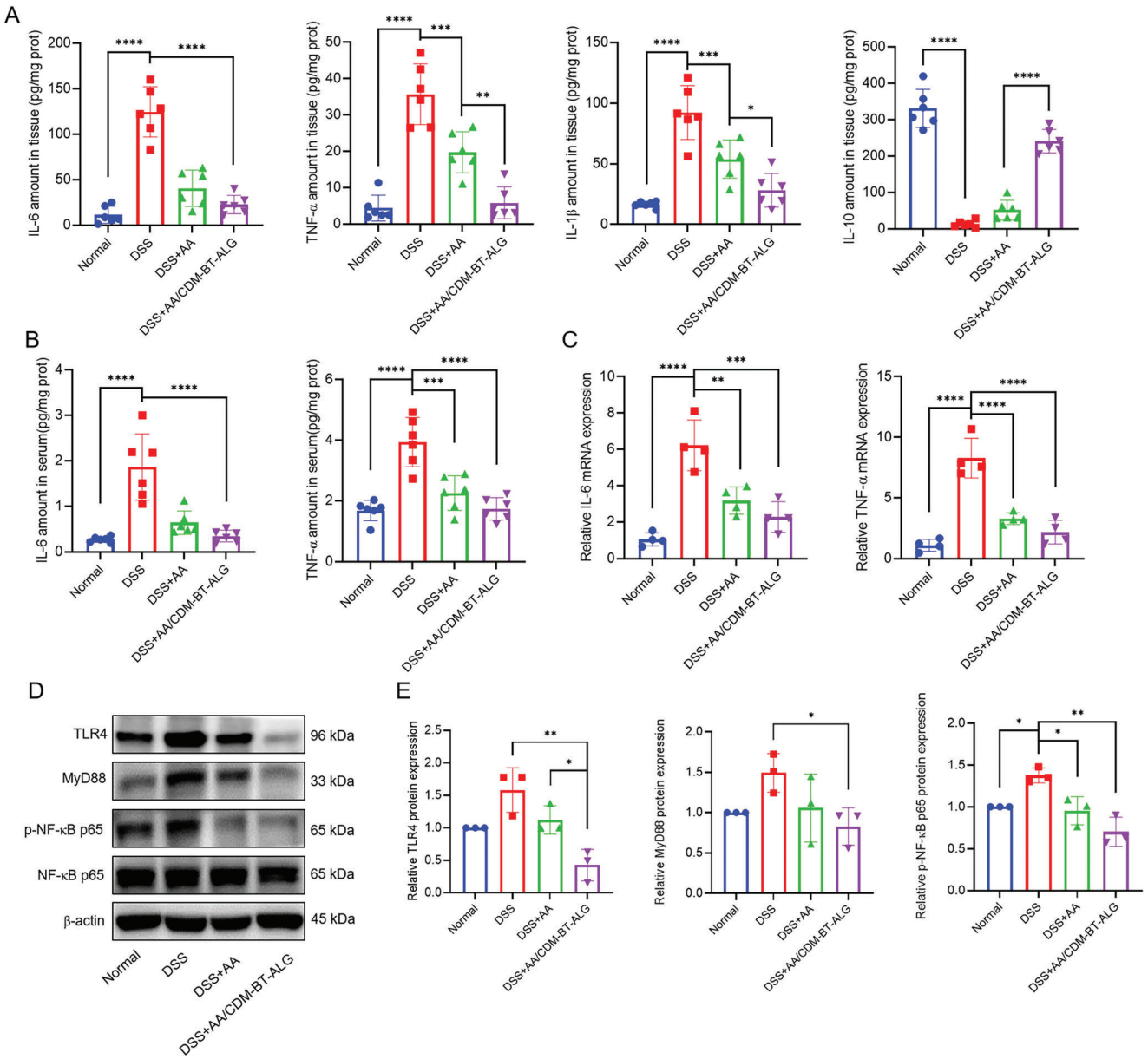

Figure 7. Effect of AA/CDM-BT-ALG on inflammatory cytokine and protein expressions after UC treatment. Colonic inflammatory cytokine changes in A) colonic tissues and B) serum were analyzed by ELISA ($n = 6$). (C) IL-6 and TNF-α mRNA expressions in the colon samples were analyzed by RT-PCR ($n = 4$). D) Western blot results and E) subsequent quantification of TLR4/MyD88/NF-κB protein expression ($n = 3$). Each point represents the mean ± SD. * $p < 0.05$; ** $p < 0.01$; *** $p < 0.001$; **** $p < 0.0001$.

group significantly improved goblet cell reduction and mucous integrity recovery.

Reduction of tight junction proteins, including ZO-1 and Claudin-1, increases intestinal permeability, leading to colonic barrier dysfunction.[43,44] Therefore, mucosal healing is becoming increasingly important in treating UC patients. Figure 6I–J presents that ZO-1 and Claudin-1 immunohistochemical staining showed the weakest immune response in the model group, possibly due to intestinal mucosal barrier destruction. Additionally, ZO-1 and Claudin-1 expressions in the AA/CDM-BT-ALG group were significantly increased, which proved to have a protective effect on the intestinal barrier of UC mice.

3.11. Infiltration of Neutrophils and Macrophages in the Colon

Immunofluorescent staining of neutrophils and macrophages in the colon was performed to assess the damage extent of colitis. MPO, a hydrogen peroxide oxidoreductase, is an essential marker for detecting the severity of mucosal neutrophil infiltration.[45] Therefore, immunofluorescence staining was used to assess MPO activity in colon samples to determine whether AA and AA/CDM-BT-ALG reduce neutrophil infiltration during DSS colitis. Representative images are shown in Figure 6K. Colon sections of healthy mice revealed no evidence of neutrophil infiltration into the mucosa, stating the absence of colitis.

However, neutrophil infiltration of the mucosa was abundant in the colon sections of DSS mice, suggesting severe colitis. Furthermore, neutrophil infiltration in the colonic mucosa of mice in the treatment groups was significantly reduced compared to untreated mice. Conversely, neutrophil infiltration in the AA/CDM-BT-ALG group was significantly reduced compared to the AA group, revealing that the targeted microspheres can improve the therapeutic effect of colitis.

Figure 6I shows macrophage infiltration in each administration group. F4/80 fluorescence was the strongest in DSS mice colon tissue, indicating many macrophage infiltrations and severe inflammation. After AA treatment, the red fluorescence became weaker, indicating that the number of macrophages decreased and the inflammation was relieved. However, the number of macrophages in AA/CDM-BT-ALG treated mice was further reduced, indicating a significant inflammation recovery consistent with neutrophil immunofluorescence findings.

3.12. Down-Regulation of the Inflammatory Factors

The levels of pro-inflammatory cytokines in colon tissue and serum were determined by ELISA to evaluate the infiltration of neutrophils and macrophages in the colon samples of each group. **Figure 7**A depicts that IL-6, TNF-α, and IL-1β were significantly up-regulated in the colon tissue of colitis mice compared to the controls, while IL-10 showed a significant down-regulation ($p < 0.0001$). The inflammatory factors in the free AA group were alleviated compared to the model group. Additionally, these levels in the AA/CDM-BT-ALG-treated group were significantly changed compared to untreated UC mice ($p < 0.001$). Moreover, IL-6 and TNF-α levels in serum samples of each group were consistent with those in colon tissue (Figure 7B). Compared to the model group, these levels were significantly reduced after AA/CDM-BT-ALG treatment ($p < 0.001$).

The study utilized RT-PCR to detect IL-6 and TNF-α gene expression levels in the colon samples (Figure 7C). These mRNA levels were significantly inhibited by free AA and were further reduced by AA/CDM-BT-ALG treatment ($p < 0.001$ or $p < 0.0001$). The inflammatory cytokine gene expression levels showed that our prepared calcium ALG microspheres protected animals against colitis effectively and safely.

3.13. In Vivo Anti-Inflammation by Inhibiting the TLR4/MyD88/NF-κB Signaling Pathway

To further investigate the AA/CDM-BT-ALG mechanism in alleviating colitis in mice, representative proteins, including TLR4, MyD88, and NF-κB p65, were evaluated by Western blotting (Figure 7D). Compared to the normal group, TLR4, MyD88, and p-NF-κB p65 protein expressions in the colon tissue of the model group increased. However, the AA/CDM-BT-ALG microspheres significantly reduced these protein expressions ($p < 0.05$ or < 0.01). Collectively, AA/CDM-BT-ALG has a reliable inhibitory impact on the TLR4/MyD88/NF-κB signaling pathway, related to its anti-inflammatory influence on DSS-induced colitis in mice.

4. Conclusion

Herin, we designed a nano-in-micro drug delivery strategy that dual-targets macrophages and intestinal epithelium for delivering the drugs specifically to the inflammatory colon of UC. The AA/CDM-BT-ALG targeting effect was verified in vitro and in vivo. In vitro, experimental results indicated that adding calcium ALG shell to nanocarriers could protect the drug from the acidic media and release it in the intestinal environment, with pH-sensitive properties. After oral administration of fluorescence-labeled microspheres to mice, the fluorescence accumulated in the colon site, verifying that AA/CDM-BT-ALG targets colonic inflammation. In vivo experiments showed that the therapeutic effect of AA/CDM-BT-ALG on mice with colitis was significantly better than that of AA. Furthermore, AA/CDM-BT-ALG can downregulate inflammatory cytokines in colon tissue and serum. The anti-inflammatory mechanism is related to TLR4/MyD88/NF-κB pathway inhibition. Eventually, our findings suggest that AA/CDM-BT-ALG may be an effective strategy for UC-targeted drug delivery. These results added to the current understanding of nanoparticle oral drug delivery systems to treat UC and other gastrointestinal diseases.

Supporting Information

Supporting Information is available from the Wiley Online Library or from the author.

Acknowledgements

This work was supported by the Natural Science Foundation of Zhejiang Province, China (LQ22H300009), Zhejiang Medical Science and Technology Project (2022KY729 and 2023KY086), and the Basic Scientific Research Project of Hangzhou Medical College (KYYB202108).

Conflict of Interest

The authors declare no conflict of interest.

Data Availability Statement

The data that support the findings of this study are available from the corresponding author upon reasonable request.

Keywords

asiatic acid, inflammation targeting, nano-in-micro structure, oral drug delivery, ulcerative colitis

Published online:

[1] X. Yan, L. Meng, X. Zhang, Z. Deng, B. Gao, Y. Zhang, M. Yang, Y. Ma, Y. Zhang, K. Tu, M. Zhang, Q. Xu, *Mol. Ther.* **2023**, *31*, 1383.
[2] S. Gou, Y. Huang, Y. Wan, Y. Ma, X. Zhou, X. Tong, J. Huang, Y. Kang, G. Pan, F. Dai, B. Xiao, *Biomaterials* **2019**, *212*, 39.
[3] R. Ungaro, S. Mehandru, P. B. Allen, L. Peyrin-Biroulet, J. F. Colombel, *Lancet* **2017**, *389*, 1756.

[4] M. F. Neurath, *Nat. Rev. Gastroenterol. Hepatol.* **2017**, *14*, 269.
[5] Y. Ma, J. Zhao, L. Cheng, C. Li, X. Yan, Z. Deng, Y. Zhang, J. Liang, C. Liu, M. Zhang, *Carbon* **2023**, *204*, 526.
[6] S. Hua, E. Marks, J. J. Schneider, S. Keely, *Nanomedicine* **2015**, *11*, 1117.
[7] M. Zhang, D. Merlin, *Inflamm Bowel Dis* **2018**, *24*, 1401.
[8] B. Xiao, Z. Xu, E. Viennois, Y. Zhang, Z. Zhang, M. Zhang, M. K. Han, Y. Kang, D. Merlin, *Mol. Ther.* **2017**, *25*, 1628.
[9] J. Zhang, Y. Zhao, T. Hou, H. Zeng, D. Kalambhe, B. Wang, X. Shen, Y. Huang, *J Control Release* **2020**, *320*, 363.
[10] P. R. Taylor, S. Gordon, L. Martinez-Pomares, *Trends Immunol.* **2005**, *26*, 104.
[11] M. Gröger, W. Holnthoner, D. Maurer, S. Lechleitner, K. Wolff, B. B. Mayr, W. Lubitz, P. Petzelbauer, *J. Immunol.* **2000**, *165*, 5428.
[12] G. K. Sinhmar, N. N. Shah, S. U. Rawal, N. V. Chokshi, H. N. Khatri, B. M. Patel, M. M. Patel, *Artif Cells Nanomed Biotechnol* **2018**, *46*, 565.
[13] S. Qi, R. Luo, X. Han, W. Nie, N. Ye, C. Fu, F. Gao, *ACS Appl. Mater. Interfaces* **2022**, *14*, 50692.
[14] Z. Zhang, S. Li, H. Cao, P. Shen, J. Liu, Y. Fu, Y. Cao, N. Zhang, *Food Funct.* **2019**, *10*, 422.
[15] T. Minko, P. V. Paranjpe, B. Qiu, A. Lalloo, R. Won, S. Stein, P. J. Sinko, *Cancer Chemother. Pharmacol.* **2002**, *50*, 143.
[16] S. Ramanathan, S. Pooyan, S. Stein, P. D. Prasad, J. Wang, M. J. Leibowitz, V. Ganapathy, P. J. Sinko, *Pharm. Res.* **2001**, *18*, 950.
[17] M. Liu, X. Song, Y. Wen, J. L. Zhu, J. Li, *ACS Appl. Mater. Interfaces* **2017**, *9*, 35673.
[18] Y. Cao, K. Cheng, M. Yang, Z. Deng, Y. Ma, X. Yan, Y. Zhang, Z. Jia, J. Wang, K. Tu, J. Liang, M. Zhang, *J. Nanobiotechnol.* **2023**, *21*, 21.
[19] S. H. Dong, Y. W. Liu, F. Wei, H. Z. Tan, Z. D. Han, *Biomed. Pharmacother.* **2017**, *89*, 1297.
[20] J. W. Lee, H. A. Park, O. K. Kwon, Y. G. Jang, J. Y. Kim, B. K. Choi, H. J. Lee, S. Lee, J. H. Paik, S. R. Oh, K. S. Ahn, H. J. Lee, *Int. Immunopharmacol.* **2016**, *39*, 208.
[21] M. F. Nagoor Meeran, S. N. Goyal, K. Suchal, C. Sharma, C. R. Patil, S. K. Ojha, *Front. Pharmacol.* **2018**, *9*, 892.
[22] Z. Li, X. Xiao, M. Yang, *Inflammation* **2016**, *39*, 1642.
[23] H. Lv, Z. Qi, S. Wang, H. Feng, X. Deng, X. Ci, *Front Immunol* **2017**, *8*, 785.
[24] Y. W. Zhang, L. L. Tu, Y. Zhang, J. C. Pan, G. L. Zheng, L. N. Yin, *Drug Delivery* **2021**, *28*, 2534.
[25] W. Xiao, W. Jiang, K. Li, Y. Hu, S. Li, L. Zhou, R. Wan, *Am. J. Transl. Res.* **2017**, *9*, 3842.
[26] L. F. Chassaud, B. J. Fry, D. R. Hawkins, J. D. Lewis, I. P. Sword, T. Taylor, D. E. Hathway, *Prog Drug Res* **1971**, *21*, 1379.
[27] X. C. Zheng, S. H. Wang, *J. Chromatogr. B Anal. Technol. Biomed. Life Sci.* **2009**, *877*, 477.
[28] Y. W. Zhang, L. L. Tu, Z. Tang, Q. Wang, G. L. Zheng, L. N. Yin, *Pharm. Dev. Technol.* **2021**, *26*, 943.
[29] S. Wirtz, V. Popp, M. Kindermann, K. Gerlach, B. Weigmann, S. Fichtner-Feigl, M. F. Neurath, *Nat. Protoc.* **2017**, *12*, 1295.
[30] H. Ali, B. Weigmann, M. F. Neurath, E. M. Collnot, M. Windbergs, C. M. Lehr, *J. Control Release* **2014**, *183*, 167.
[31] J. Gu, S. Su, J. Guo, Y. Zhu, M. Zhao, J. A. Duan, *J. Pharm. Pharmacol.* **2018**, *70*, 268.
[32] X. Zhang, Y. Ma, L. Ma, M. Zu, H. Song, B. Xiao, *Carbohydr. Polym.* **2019**, *223*, 115126.
[33] F. E. Chen, H. Q. Jia, X. X. Chen, H. F. Dai, B. Xie, Y. Y. Kuang, J. F. Zhao, *Chem. Pharm. Bull.* **2005**, *53*, 743.
[34] H. Nosrati, P. Barzegari, H. Danafar, H. K. Manjili, *Artif Cells Nanomed. Biotechnol.* **2019**, *47*, 104.
[35] A. P. Bagre, K. Jain, N. K. Jain, *Int. J. Pharm.* **2013**, *456*, 31.
[36] A. D. Vadlapudi, R. K. Vadlapatla, A. K. Mitra, *Curr. Drug Targets* **2012**, *13*, 994.
[37] U. P. Singh, N. P. Singh, E. A. Murphy, R. L. Price, R. Fayad, M. Nagarkatti, P. S. Nagarkatti, *Cytokine* **2016**, *77*, 44.
[38] J. Erbach, F. Bonn, M. Diesner, A. Arnold, J. Stein, O. Schröder, A. Aksan, *J. Clin. Med.* **2022**, *11*, 1118.
[39] T. Kuroishi, Y. Endo, K. Muramoto, S. Sugawara, *J Leukoc Biol.* **2008**, *83*, 912.
[40] M. A. Taemeh, A. Shiravandi, M. A. Korayem, H. Daemi, *Carbohydr. Polym.* **2020**, *228*, 115419.
[41] S. Li, H. Zhang, K. Chen, M. Jin, S. H. Vu, S. Jung, N. He, Z. Zheng, M. S. Lee, *Drug Delivery* **2022**, *29*, 1142.
[42] M. Hoffmann, U. Schwertassek, A. Seydel, K. Weber, W. Falk, S. Hauschildt, J. Lehmann, *Lab. Anim.* **2018**, *52*, 240.
[43] G. Wang, Q. Li, D. Chen, B. Wu, Y. Wu, W. Tong, P. Huang, *Theranostics* **2019**, *9*, 6191.
[44] J. Wang, C. Zhang, C. Guo, X. Li, *Int. J. Mol. Sci.* **2019**, *20*, 5751.
[45] Y. J. Jin, S. Kang, P. Park, D. Choi, D. W. Kim, D. Jung, J. Koh, J. Jeon, M. Lee, J. Ham, J. H. Seo, H. R. Jin, Y. Lee, *ACS Appl. Mater. Interfaces* **2017**, *9*, 19161.